

Development and modelling of a new type of sensor for detecting current transients for power system protection



Amila Pathirana*, C.K.G. Piyadasa, Athula D. Rajapakse

Department of Electrical and Computer Engineering, University of Manitoba, Winnipeg, Manitoba, Canada

ARTICLE INFO

Keywords:

Transient based protection
Transient polarity identification
Ferrite core modelling

ABSTRACT

A new type of sensor is proposed to detect high frequency transients in currents and their initial polarities. The proposed sensing system replaces both high frequency signal sampling and processing by a simple detection coil wound on a ferrite core and an analogue electronic circuit. It is verified through laboratory experiments that transient occurrence, occurrence time, and initial transient polarity can be determined accurately. A detailed model of the sensor, including the dynamic hysteresis characteristics of the ferrite core, is developed and implemented on an electromagnetic transient simulation software, and verified through experimental measurements. Application of the developed model to simulate a transient current polarity comparison based protection scheme is demonstrated. The versatility of the proposed sensor compared to common digital signal processing based approaches, namely discrete wavelet transform and mathematical morphology, is highlighted using experimental waveforms.

1. Introduction

Conventional power system protection algorithms that operate on the phasor values of the power frequency currents and voltages have served well over many decades, but with the increasing penetration of inverter interfaced renewable energy sources [1], they are facing many challenges, mainly arising from lack of fault current contributions from inverter-interfaced sources during network faults. These problems are well documented for distribution networks with Distributed Energy Resources (DERs) [2–5], but similar problems are appearing in transmission networks as well with the interconnection of large wind and solar farms [3,4]. Thus there is renewed interest in transient based and time domain protection methods [6–9] as these techniques are less dependent on the sustained fault currents. Some commercial protection relays based on time domain principles are emerging [10]. Protection using transient signals has other advantages such as fast operation and immunity to current transformer (CT) saturation [11,12]. There are several different approaches for transient based protection: travelling wave based protection [9,13], transient directional comparison [14,15], and differential schemes based on derived quantities such as transient energy [8]. Travelling wave technique requires precise detection of travelling wave arrival times at the measurement location [16], while transient directional comparison techniques need determination of the polarity of the initial transient [14]. Differential techniques such as the method presented in [15] usually require comparison

of signal components in a specific (high) frequency band. The method proposed in [6] does not require any signal comparisons but relies on polarity of the transient signals.

The general approach used in the transient based methods is to sample the input voltage or current signals at a frequency much higher than the sampling rates used in phasor based relays. Then various signal processing techniques, for example wavelet transform [14], S-transform [8], and mathematical morphology [9,17,18] are used to extract the required signals. This approach generally requires high frequency, high precision sampling, and thus expensive analogue to digital (A/D) converters [9,14]. Furthermore, signal noise affects the sensitivity and performance. In some cases, the limited bandwidth of conventional CTs and voltage transformers (VTs) can become critical. Information on the practical implementation issues and limitations related to signal acquisition and conditioning are rare in the published literature [12].

Conventional current transformers (CTs) used for current measurements in power networks may not be adequate for measuring high frequency transients due to limited bandwidth, magnetic saturation under fault current conditions and dispersion of transient signal due to secondary leakage inductance (typically several hundreds of μH), depending on the interested range of frequency [11,19]. Rogowski coils have been utilized for power frequency and transient current measurements due to their high bandwidth, linearity, and ability to measure large currents [20]. However, if it is required to obtain a measurement directly proportional to the primary current, Rogowski coil

* Corresponding author.

E-mail address: umkarasi@myumanitoba.ca (A. Pathirana).

requires an integrator since the output from a Rogowski coil is proportional to the rate of change of current going through it. Apart from that, since there are no magnetic materials in the flux path, output voltages are quite low relative to the conventional CTs. Few authors have proposed the use of open circuited coils similar to Rogowski coils but wound on ferrite cores [21–23] for transient detection. These publications however, provide only limited insight into theoretical aspects and mathematical modelling.

Some transient based protection methods [6,13,14] and fault location applications [24] only considers the initial transient polarity or the time of arrival of the transmitted/reflected travelling waves. For this kind of applications, accurate measurement of the current waveform is not necessary, but accurate detection of high frequency transients with minimal rise time is essential. In this paper, a novel sensor and signal processing circuitry suitable for the above type of applications is proposed. The proposed sensing system replaces both high frequency signal sampling and processing, and relies on a simple detection coil wound on a ferrite core as proposed in [21]. Application of the proposed sensor for transient directional comparison type protection is focused in the paper, but it can be easily modified for using in travelling wave based and differential schemes. A main contribution of the paper is the development of a model for the sensor so that it can be represented in electromagnetic transient (EMT) simulations, which are widely used for investigating power system protection applications. The developed model is extensively verified using laboratory measurements. Finally, the advantages of the proposed sensor over the digital signal processing approaches is illustrated.

2. Arrangement and operation of the new current transient detector

Arrangement of the proposed new sensor for detecting current transients and their polarities is illustrated in Fig. 1. The primary element in the sensor is a coil wound on a ferrite core. A clip-on type core is preferred, because then the sensing coil can be easily clipped-on to the conductor that carries the input current. The coil, which consists of only few turns, is kept open circuited. The induced voltage on the coil is fed to the second stage of the sensor, which is a protection circuit containing a fuse and a surge suppressor. This protection circuit prevents damage to the low voltage electronics circuits of the relay due to high voltages that can be induced on the essentially open circuit coil. The third stage of the sensor is a passive high pass filter to remove the power frequency current and lower order harmonics. If desired, an optional low pass filter can be included after the high pass filter to remove unwanted noise.

The design of the ferrite core is such that a slight saturation is tolerated under power frequency currents. Thus the induced voltages can have a distorted waveform, resulting in significant amount of lower

order harmonics. The cut-off frequency of the high pass filter was set to 1 kHz to block the power frequency signal and these lower order harmonics. The optional low pass filter cut-off frequency was set to 200 kHz filter out any noise. If this low pass filter is not included, the upper limit of the frequency range of the sensing system is limited by the frequency response of the ferrite core coil. Since the coil is designed with only a few secondary turns, it has a very small self-inductance and capacitance, and therefore the upper limit of coil bandwidth is imposed by the frequency response of the permeability of ferrite core. This limit is in the range of several MHz for typical ferrite materials [24].

The next stage of the sensor has two fast comparators, one with a positive threshold and the other with a negative threshold. The comparator with positive threshold detects transients with positive polarity and the one with the negative threshold detects transients with negative polarity. These thresholds need to be set well above the signal noise that is present under normal conditions. In this implementation, 100% of the noise was considered as the threshold. The last stage of the sensor is a resettable bistable latch and logic to allow only the output corresponding to the initial polarity to go high. When a transient is of oscillatory nature, both positive and negative comparators will trigger one after the other, this logic blocks the second signal. The output of the sensor can be used to detect the time of transient as well as its initial polarity precisely. Once a transient is detected, the latch need to be reset to make the sensor ready for detecting the next transient.

The input current can be either a current flowing in a high voltage conductor or a current on the secondary of a conventional current transformer (CT). When using the sensor for directly measuring the primary currents in a high voltage conductor, adequate insulation must be provided between the conductor and the ferrite core coil, similar to a conventional CT. Furthermore, coil parameters like number of turns should be adjusted accordingly while rest of the circuit can be used without any adjustments except thresholds. In this implementation we included the ferrite core coil in the secondary of primary CT considering the practical considerations but it is preferred to include the coil along line current if possible. When the sensor is used on the secondary side of a CT, insulation requirements are minimal, and the whole sensor can be mounted inside a protection relay. However, in this case, the frequency range of the detectable transients will be constrained by the bandwidth of the conventional CT, which can be limited to about 20 kHz [19].

The operating principle of the ferrite core coil sensor is similar to a Rogowski, and its output voltage is proportional to the rate of change of the input current when operating in the linear region. However, to design a coil that is operating in the linear region requires a ferrite core with a large cross section, making the sensor bulky and expensive. As it will be shown later, this is not necessary, as the objective is to detect only transients: the transients can be successfully detected even when the core is in saturation. When the core is saturating, the output

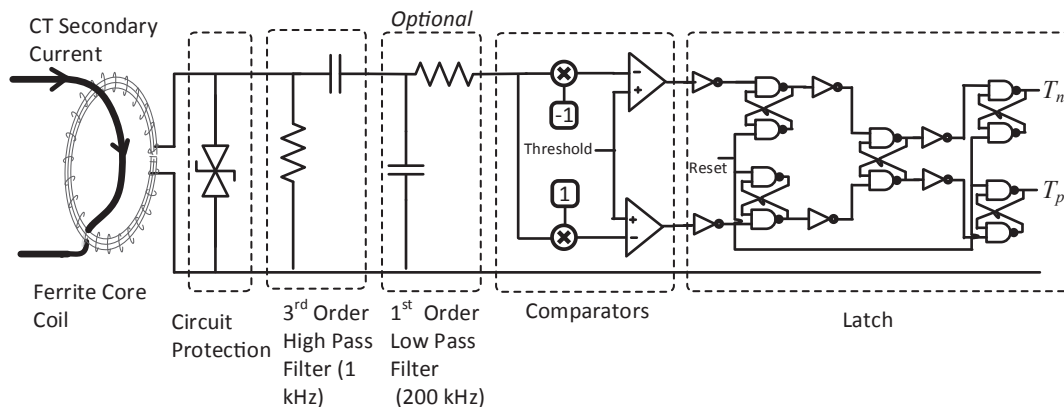


Fig. 1. Current transient detection sensor.

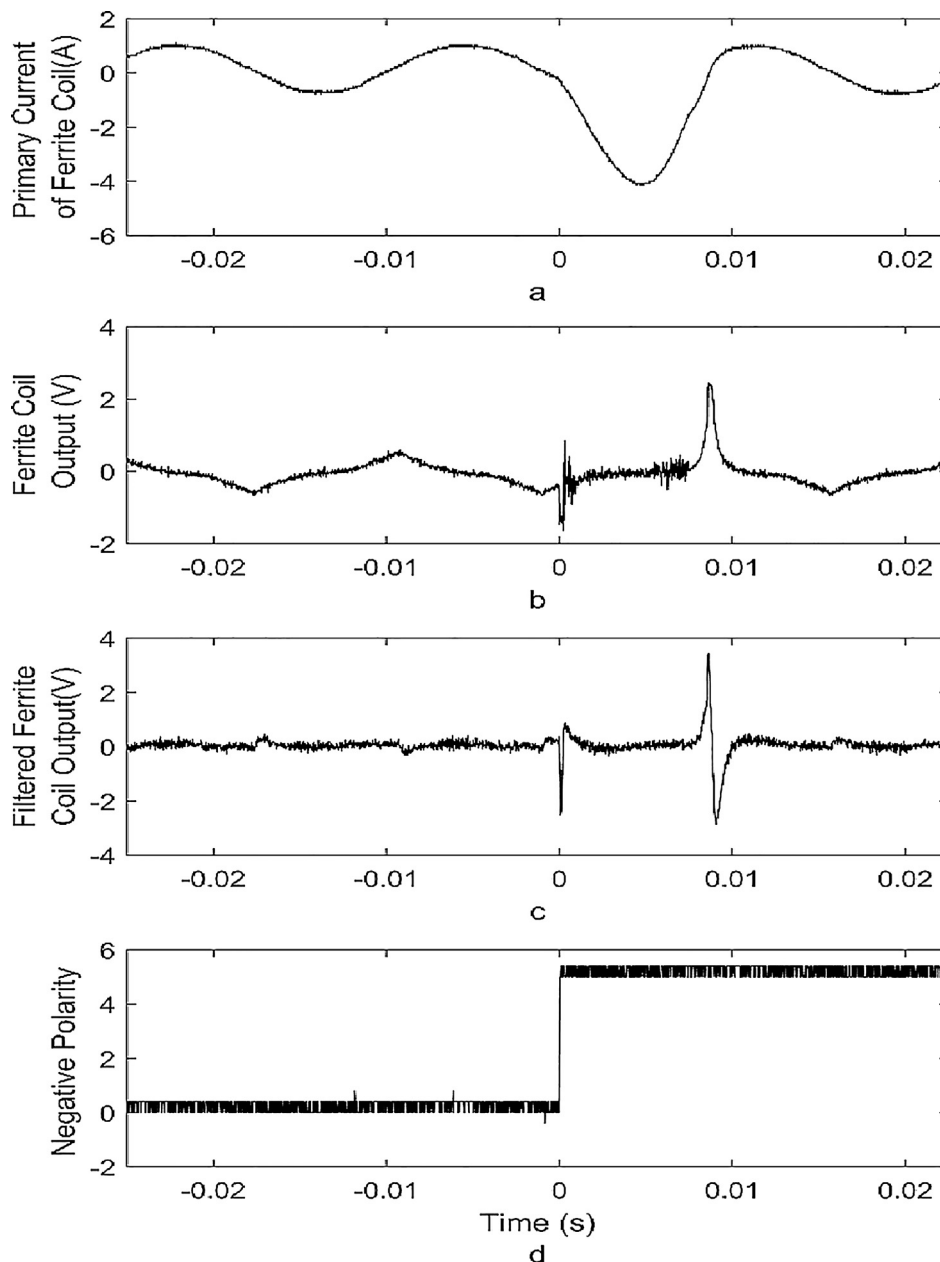


Fig. 2. Response of the sensor for a fault current (a) input primary current, (b) ferrite core coil output voltage, (c) coil voltage after high pass filter, and (d) T_n output of latching circuit.

waveform is distorted according to the hysteresis characteristics of the ferrite core. Use of a ferrite core in the proposed sensor has many advantages. Due to higher relative permeability of ferrite, magnitude of the output voltage is several orders higher than the voltage induced on an air cored Rogowski coil. This also enables to design the sensing coil with only a few turns, thereby reducing its self-inductance. Self-inductance of the coil is main factor that limits the slew rate and the bandwidth (unless it is constrained by a conventional primary CT).

In order to understand the working of the sensor, consider Fig. 2, which shows examples of the measured signals at different stages of the proposed transient polarity detector. Fig. 2(a) shows the current in the primary circuit during a transient fault event (created on a low voltage circuit in the laboratory). The graph in Fig. 2(b) shows the output voltage of the ferrite core coil. Next the output of the ferrite core sensor is filtered using third order high pass RC filter. This filtered signal shown in Fig. 2(c) is then input to the transient detection comparators. The output of the sensor, which indicates the time of transient and its

initial polarity is shown in Fig. 2(d). Note that only the output corresponding to the negative transient is shown here, due to limited number of inputs available in the oscilloscope recording the waveforms.

Performance of a given protection algorithm is usually examined through simulations of the power system together with the protection devices, since actual field tests are prohibitive. As mentioned earlier, EMT simulation programs are used for this purpose. In this study, the well-known EMT program PSCAD is used, and its extensive master library contains most of the power system and control system component models required for the simulation. However, a model need to be developed for the ferrite core coil with saturation and hysteresis characteristics. Following section details the mathematical formulation of the ferrite core coil to be used in PSCAD simulation program.

3. Formulation of the mathematical model of ferrite core sensor

Arrangement of a open circuited ferrite core coil is shown in Fig. 3.

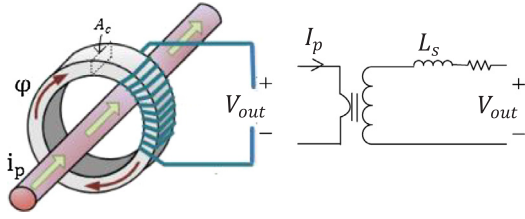


Fig. 3. Arrangement of the transient detecting sensor.

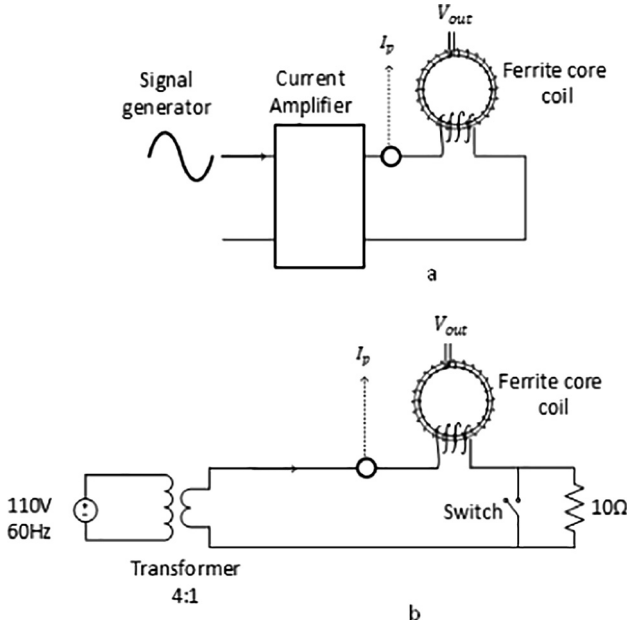


Fig. 4. Experimental setups used to validate the simulation model of ferrite core coil.

It is similar to a conventional CT (Current Transformer) in its physical arrangement, but more related to a Rogowski coil in operation. However, there are key differences from both conventional CT and Rogowski coils. The next section illustrate the steps of mathematical formulation of ferrite core coil.

3.1. Modelling of hysteresis of the ferrite core

The Jiles-Atherton (JA) theory [25] presents a quantitative model of hysteresis phenomena constructed using mathematical formulations. This model exhibits all of the main features of hysteresis such as the initial magnetization curve, saturation of magnetization, coercivity, remanence, and hysteresis loss, and therefore suitable to model the ferrite core sensor used in this study. JA theory starts to describe the hysteresis of a magnetic material by transforming the relationship between magnetic field density B and magnetic field strength H into a relationship between magnetic moment M and effective field H_e as given in (1) and (2):

$$B = \mu_0(H + M) \quad (1)$$

$$H_e = H + \alpha M \quad (2)$$

where α represents the inter-domain coupling interaction. The anhysteretic magnetization M_{an} , can be expressed in the form given in (3), where M_{Sat} is the saturation magnetization and f is an arbitrary function of the effective field.

$$M_{an} = M_{Sat}f(H_e) \quad (3)$$

JA model use a modified Langevin function to represent $f(H_e)$ as given in (4), where the parameter A is used to define the shape of the

model.

$$f(H_e) = \coth(H_e/A) - A/H_e \quad (4)$$

According to the JA theory, magnetic moment M consists of two components as shown in (5) where M_{irrev} represents the pinning of the magnetic domains by discontinuities in the material structure and M_{revs} represents the domain wall bending in an elastic manner.

$$M = M_{irrev} + M_{revs} \quad (5)$$

Then the relationship between M and H can be expressed using the differential equations given in (7) and (8) as proposed in [26], where c is called the domain flexing parameter and δ is a variable that indicates whether the magnetic field is increasing or decreasing.

$$\frac{dM}{dH} = \frac{c \frac{dM_{an}}{dH_e} + \frac{M_{an} - M}{\mu_0 \frac{\delta k - \alpha(M_{an} - M)}{1 - c}}}{1 - \alpha c \frac{dM_{an}}{dH_e}} \quad \text{for all } (M_{an} - M)\delta > 0 \quad (6)$$

$$\frac{dM}{dH} = \frac{c \frac{dM_{an}}{dH_e}}{1 - \alpha c \frac{dM_{an}}{dH_e}} \quad \text{for all } (M_{an} - M)\delta < 0 \quad (7)$$

where,

$$\delta = 1 \text{ if } \frac{dH}{dt} > 1$$

$$\delta = -1 \text{ if } \frac{dH}{dt} < 1$$

A , α , c and k are constants for the material being used, and can be determined using measured hysteresis curves and curve fitting techniques. Evaluation of these parameters is discussed in [26].

3.2. Inclusion of dynamic behaviour

The hysteresis model described by (1)–(7) is static and mainly used for describing the power frequency behaviour of ferromagnetic materials. It does not represent the frequency dependent or dynamic behaviour of hysteresis characteristics. In order to model the dynamic behaviour and the resulting variations in the energy losses in the core, JA model need to be extended. The dynamic behaviour can be included in various ways. For example, in [27], a term proportional to dB/dt is added to (2). Ref. [27] achieves the dynamic behaviour by dividing the static dM/dH by a dynamic factor proportional to dB/dt . Furthermore, in [27], it is shown that a dynamic factor proportional to dH/dt gives a better fit to experimental data than the term proportional to dB/dt . Apart from that, the natural independent variable of the data is H . Therefore, it is straightforward to adopt H as the independent variable for dynamic model rather than B .

After comparison of different approaches, it was found the latter model gives a good representation for high frequency excitations while retaining the ability to represent static magnetization. Thus, (6) and (7) were modified to incorporate dynamic behaviour as shown in (8).

$$\left(\frac{dM}{dH}\right)_{dynamic} = \frac{\left(\frac{dM}{dH}\right)_{static}}{1 + R \left|\frac{dH}{dt}\right|} \quad (8)$$

The factor R is a material property and can be determined experimentally using curve fitting with measured high frequency hysteresis curves, as discussed in [27].

3.3. EMT simulation model of the ferrite core coil

When modelling open circuited ferrite core coil in an EMT simulation program, it is necessary to determine the change in secondary voltage for a given change in primary current in each simulation time interval, Δt . Such a model can be developed from basic principles. Applying Ampere’s law to the core of the coil shown in Fig. 3, it is

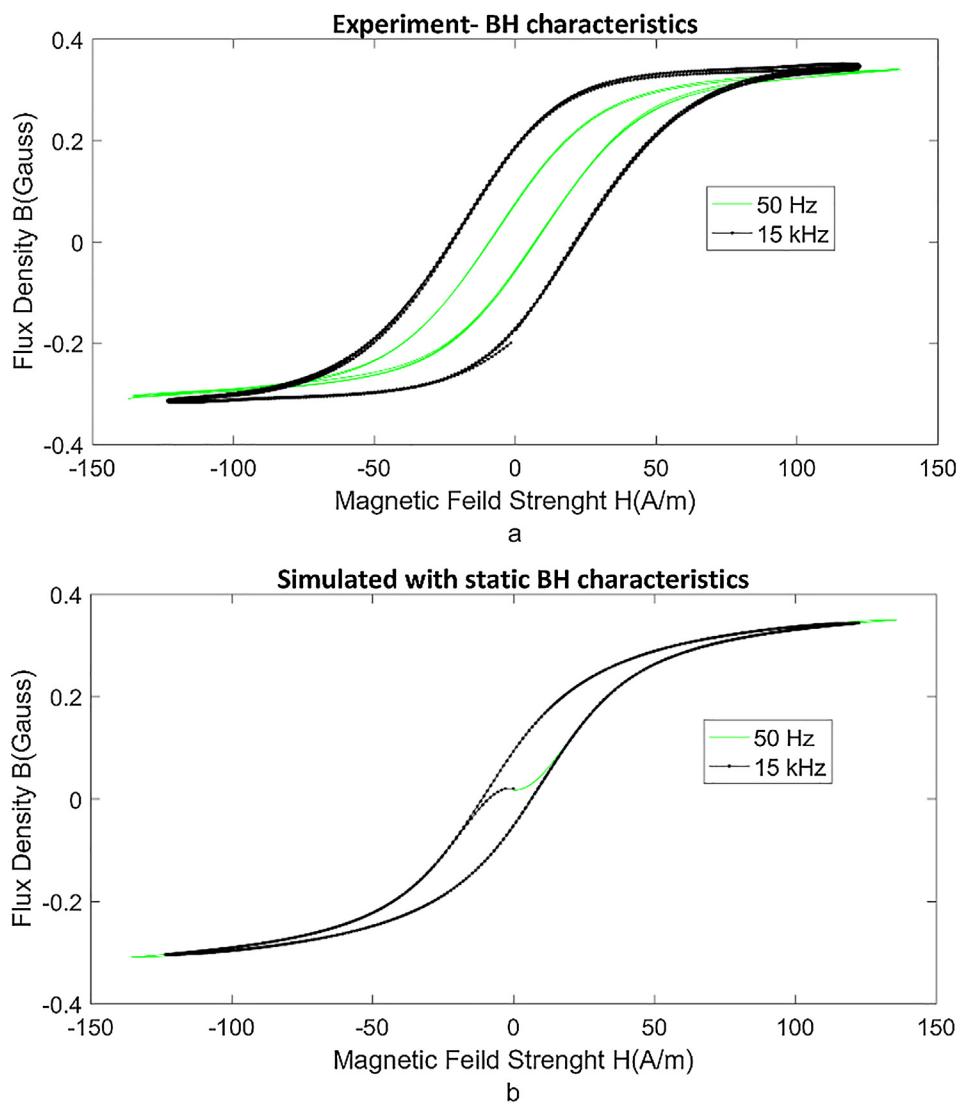


Fig. 5. (a) Experimental results illustrating the dynamic behaviour of the B-H curve (b) Simulation results with static B-H curve model.

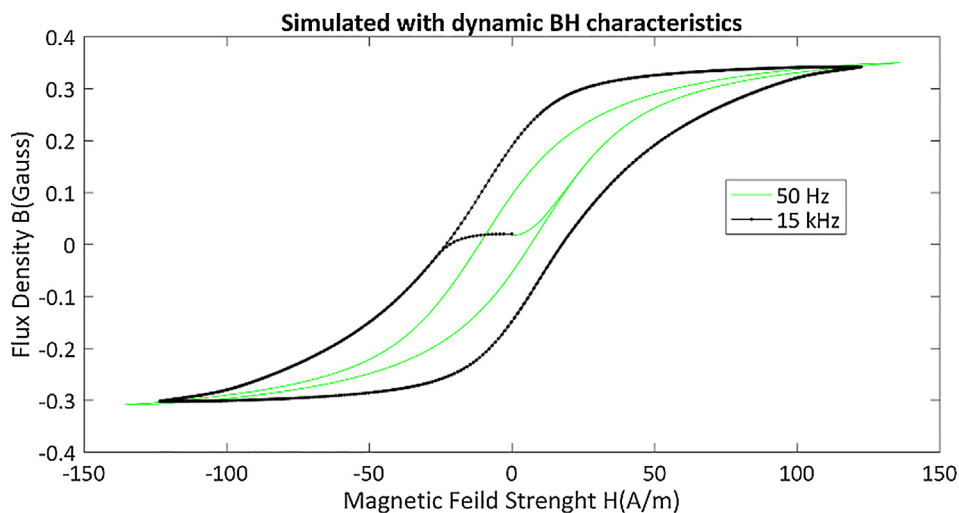


Fig. 6. Simulation results with the dynamic B-H curve model.

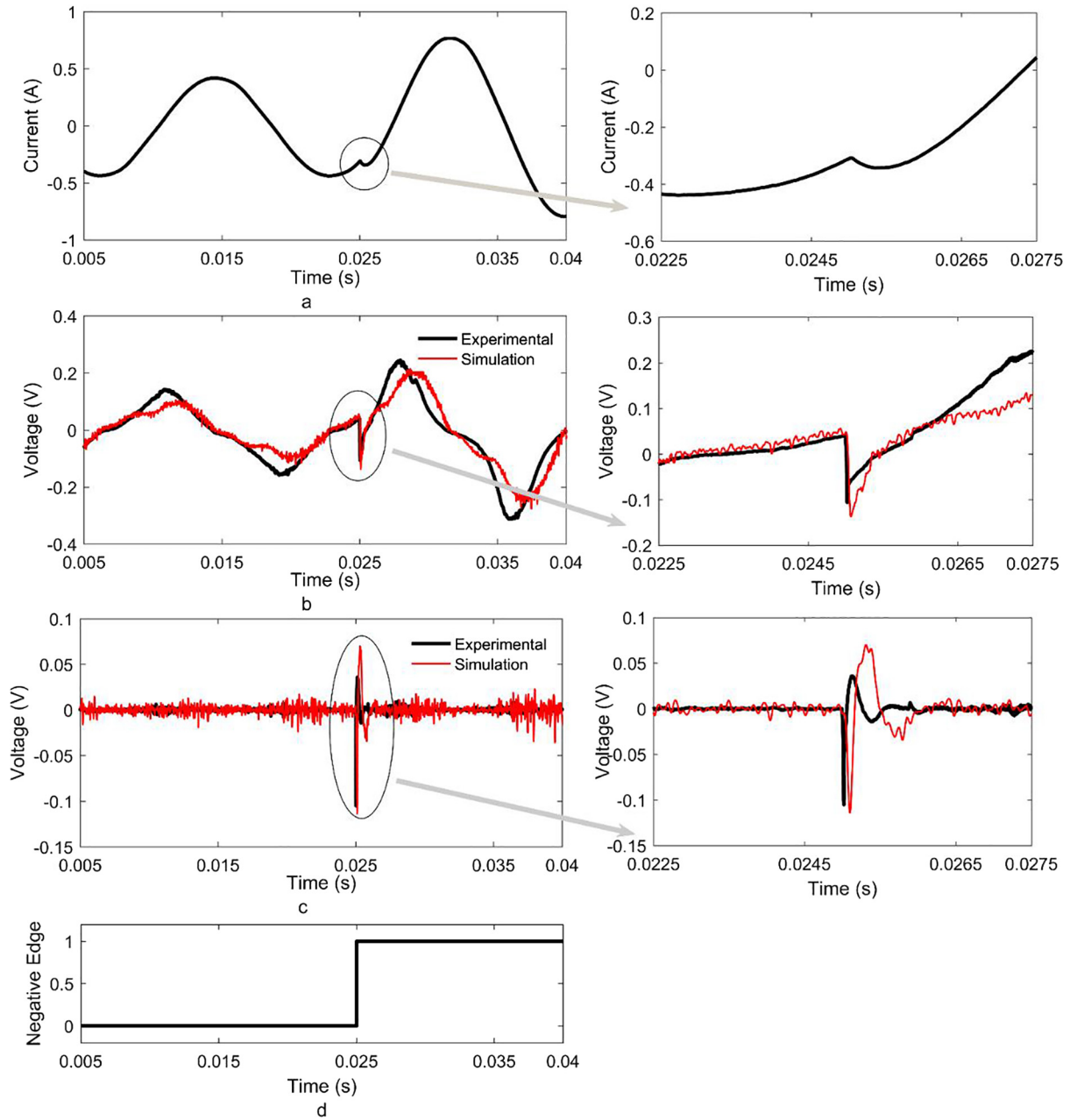


Fig. 7. The measured and simulated output voltages during a transient (a) primary current, (b) secondary coil output voltage, (c) output voltages after filtering and (d) output indicating the initial polarity and the detection of transient.

possible to show that,

$$\Delta H = \frac{N_p}{l} \Delta I_p \tag{9}$$

where N_p is the number of turns in the primary; l is the length of the flux path, ΔH is the change in magnetic field strength and ΔI_p is the change in primary current which is the excitation given to the model. In the proposed sensor, the coil output is connected to a voltage measurement circuit, thus the secondary current, I_s is assumed to be negligible. Therefore, the output voltage, V_{out} is obtained as

$$V_{out} = \frac{N_s A_c}{\Delta t} \Delta B \tag{10}$$

The value of ΔB can be calculated by solving (1)–(8), with ΔH obtained from (9). These equations are solved in each time step to determine the three unknowns ΔH , ΔM and ΔB to be used in the next time step. Finally, ΔB can be used to determine the output voltage of the

ferrite core coil according to (10). This procedure was implemented through a user-defined model in EMT simulation software PSCAD. As the model is highly nonlinear, precautions need to be taken to maintain the numerical stability by selecting appropriate simulation time step.

4. Validation of the ferrite core coil model

The formulated mathematical model of the ferrite sensor is validated using laboratory experiments. The validation consists of two parts. First in Section 4.1, dynamic behaviour of the hysteresis characteristics modelled using the proposed model is validated by comparing with experimentally obtained characteristics. The experimental setup shown in Fig. 4(a) is used to generate sinusoidal primary currents of different frequencies, using a current amplifier. The ferrite core (MnZn) used in the experiment has a cross section area of $2 \times 10^{-4} \text{ m}^2$, a mean core length of $12 \times 10^{-2} \text{ m}$, and 8 turns in the secondary coil.

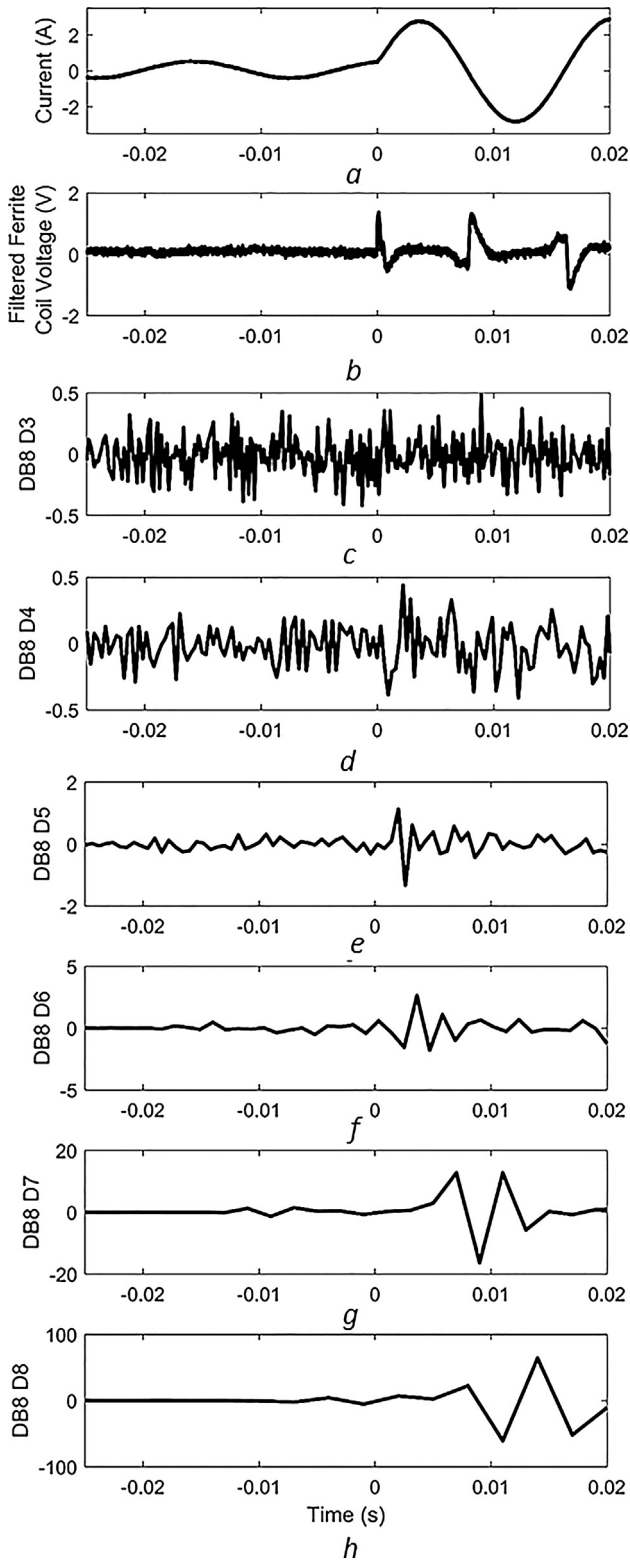


Fig. 8. Detail wavelet coefficients of DB8 mother wavelet. (a) Input current (b) Filtered ferrite coil output (c)–(g) detail wavelet coefficients of Levels 3–8.

Leakage inductance of the coil is 160 μH . The values of magnetic flux density B and field intensity H are obtained from the measured input voltage and currents using (11) and (12). The measured primary currents from the experimental setup, sampled at 40 kHz, are used as the input for the simulation model.

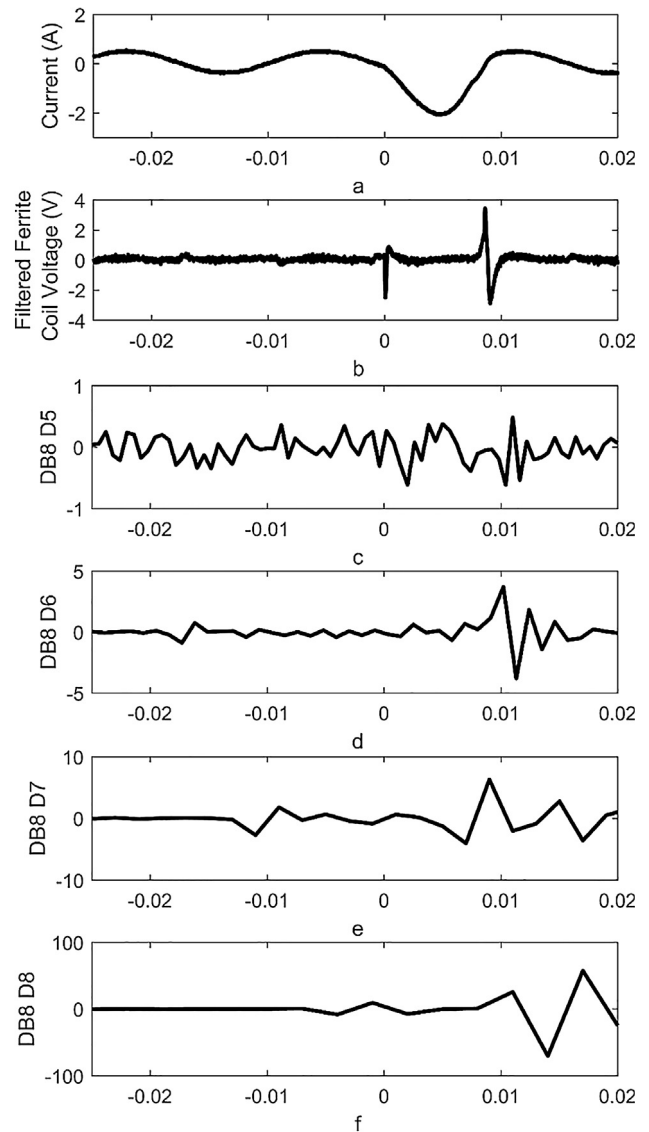


Fig. 9. Detail wavelet coefficients of DB8 mother wavelet. (a) Input current (b) Filtered ferrite coil output (c)–(f) detail wavelet coefficients of Levels 5–8.

$$H = \frac{N_p}{l} I_p \tag{11}$$

$$B = \frac{A_c}{N_s} \int V_{out} dt \tag{12}$$

In Section 4.2, the measured output voltage waveform of the same ferrite core coil for a primary current containing a transient is compared with that obtained from the model. The input to the model is again the measured primary current. In order to produce a transient current, the experimental setup shown in Fig. 4(b) is used. A primary current resembling a fault current is created by short-circuiting the output of a 120/30 V single phase transformer, by closing the load bypass switch. This approach was used because the current amplifier bandwidth is limited to 20 kHz.

4.1. Validation of dynamic B-H curve model

The designed sensor is targeted for detecting high frequency transients, and therefore, the high frequency behaviour of the core material should be correctly modelled in the simulation model. Dynamic behaviour of core is included into the model as described in the Section 3.2. Fig. 5(a) demonstrate the difference between the measured hysteresis

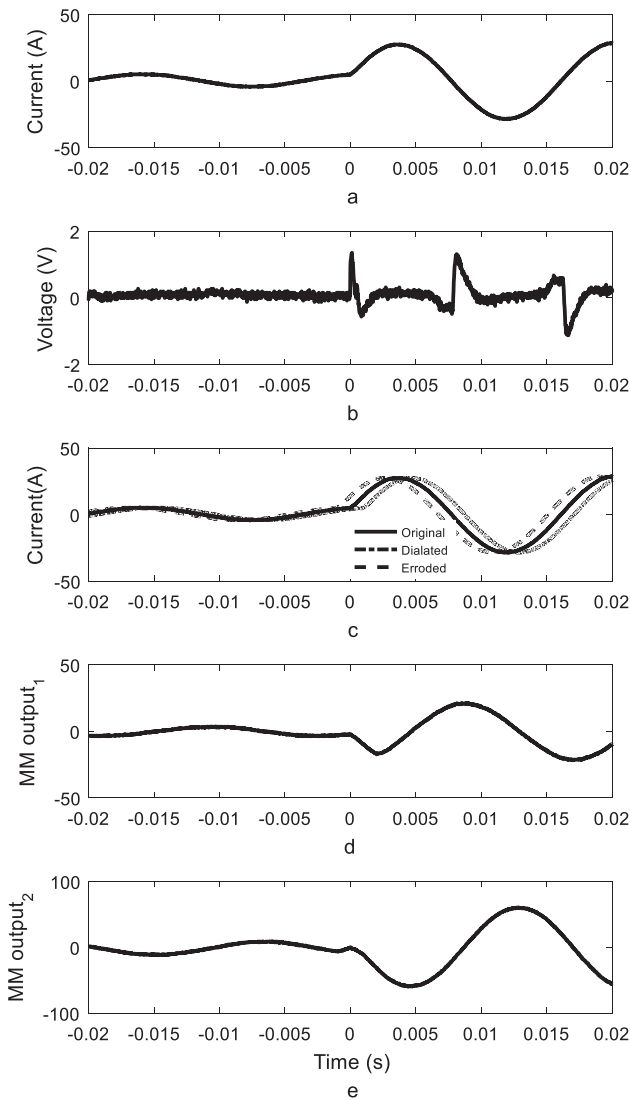


Fig. 10. Outputs of MM compared to filtered ferrite coil sensor (Case 1) (a) Input current (b) Filtered ferrite coil output (c) Dilated and eroded waveforms of original current (d) MM Output of operation proposed in [17] (e) MM Output of the operation proposed in [18].

characteristics of the ferrite core for two different frequencies. As expected, the width of the hysteresis loops increase with the frequency. Fig. 5(b) shows the hysteresis characteristics computed with the static model (i.e. without the modification given in (8)) for the two frequencies, using measured primary currents as the model inputs: the changes in the hysteresis loops with the frequency will not appear in the simulated curves. The model parameters for these curves are obtained using measurements made at 50 Hz.

Fig. 6 demonstrates B-H curves obtained with the dynamic model of hysteresis characteristics, for the same primary current inputs. Modification proposed in (8) with the dynamic factor is simple, but very effective in capturing the frequency dependent behaviour of hysteresis curves. The B-H curves in Fig. 6 are very close to those in Fig. 5, although there are some minor differences around the knee points. The factor R in (8) is evaluated by curve fitting with a high frequency B-H curve obtained at 10 kHz.

4.2. Output voltages during transients

The primary current applied to the ferrite core coil using the setup illustrated in Fig. 4(b) in this experiment is shown in Fig. 7(a). The same

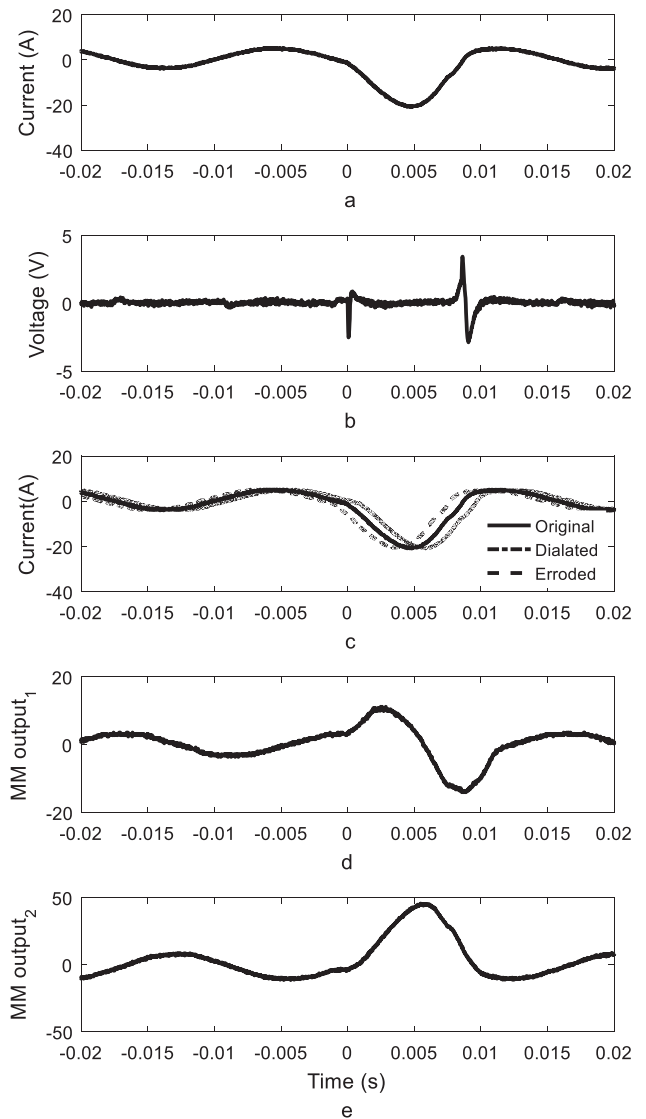


Fig. 11. Outputs of MM compared to filtered ferrite coil sensor (Case 2) (a) Input current (b) Filtered ferrite coil output (c) Dilated and eroded waveforms of original current (d) MM Output of operation proposed in [17] (e) MM Output of the operation proposed in [18].

current is applied as the input to the simulation model. The output voltage of the secondary coil measured from the experiment is compared with that computed using the proposed simulation model in Fig. 7(b). It can be seen that the simulation model reasonably well captures the coil output voltage during the transient, although there are some minor differences in the subsequent period. When used for transient based protection applications, often the regular power frequency component is filtered out using a high pass filter. The measured and computed voltages after high pass filtering are shown in Fig. 7(c). The model captures the main features of the transient such as the initial polarity and peak magnitude fairly well. Using a comparator circuit initial polarity can be identified as shown in Fig. 7(d). These results also confirms that the approach proposed for selecting the comparator thresholds is reasonable.

5. Comparison of the proposed transient detection method with digital signal processing approaches

In this section proposed sensor output is compared with the Wavelet transform and Mathematical Morphology methods, two techniques

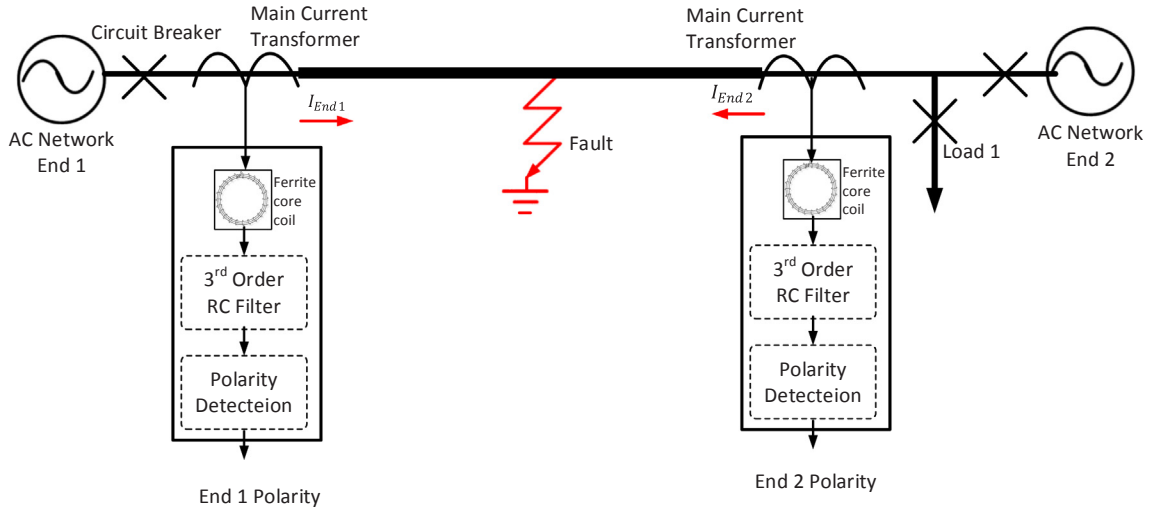


Fig. 12. Test network model and transient polarity comparison protection simulated in PSCAD for demonstrating application of the simulation model.

commonly proposed in literature for disturbance detection.

5.1. Wavelet transform

Wavelet transform is often proposed for extracting transients from signals in literature [14,18,28]. The wavelet transformation of a sampled function is given as

$$WT_{\psi}f(s,\tau) = \sum_k f(k)\psi_{s,\tau}^*(k) \quad (13)$$

where $\psi_{s,\tau}^*$ is a dilated (scaled) and translated (shifted) version of the mother wavelet function. The wavelet transform can be continuous or discrete, depending on the way the dilation and translation parameters are selected. Wavelet transform decomposes the signal into a family of frequency bands. The value of s in (13) is known as the level of wavelet coefficients and corresponds to a particular frequency band, with the lowest level corresponding to the highest frequency band. These high-frequency components are known as detailed wavelet coefficients. Discrete wavelet coefficients corresponding to different scales can be extracted directly from ‘Mallat tree algorithm’ implementation of the wavelet transform [27].

In order to compare the performance of the proposed method of transient and its polarity detection, the output waveforms of the ferrite sensor are compared with the wavelet transform coefficients of the primary current. Experiments with different mother wavelets showed the DB8 mother wavelet is best for this application. For the input current waveform shown in Fig. 8(a), DB8 reconstruction wavelet coefficients of different detailed levels (D3-D8) are plotted in Fig. 8(c)–(h). The detail coefficients below level 4 were just noise. The detail wavelet coefficients of level 5 and 6 appears to capture the transient for this waveform. The detail coefficients above level 6 just show the low frequency variations (65–265 Hz) in the current.

In Fig. 9, detailed wavelet coefficients (D5-D8) are shown for a different input current. This is corresponding to a fault happening close to the current zero crossing, thus the resulting current surge is minimal. For this case, any of the detailed wavelet coefficients do not properly capture the initial transient (what is visible in Level 6 is the transient resulting when the temporary fault is cleared. However, the filtered ferrite core coil output voltage shows a clear spike corresponding to the initial transient as well, which is barely visible in the input current.

5.2. Mathematical morphology

Mathematical Morphology (MM) is another technique, which has been used for extracting the information of high frequency signals

related to signal disturbances. Similar to Wavelet transform, MM is also focused on the shape and size of signals in the time domain and needs a smaller information window [9]. In MM, a Structural element (SE) is used to extract the necessary signal properties. MM consists of two basic operators called erosion and dilation. Based on those primary operators, secondary operators such as opening and closing are defined [18].

Following formulation of MM detailed in [18] is used to compare the effectiveness of the method with proposed ferrite coil sensor. Assuming that $f(n)$ is the input signal as defined discrete function with amplitudes $D_f = \{0,1,2,\dots,n-1\}$ and $g(m)$ is an SE defined with amplitudes $D_g = \{0,1,2,\dots,m-1\}$, then dilation of signal f by g is denoted by $(f \oplus g)$ and erosion of domain f by g is denoted by $(f \ominus g)$ and defined as follows:

$$f_{dil}(n) = (f \oplus g)(n) = \max\{f(n+m) + g(m)\} \quad (15)$$

$$f_{ero}(n) = (f \ominus g)(n) = \max\{f(n-m) - g(m)\} \quad (16)$$

By combining the above two operators, two other operators called opening and closing are obtained. Opening operation of signal f by g is denoted by $f \circ g$ and defined as:

$$f_{open}(n) = (f \circ g)(n) = ((f \oplus g) \ominus g)(n) \quad (17)$$

Also, the closing operation of signal f by g is denoted by $f \bullet g$ and defined as:

$$f_{close}(n) = (f \bullet g)(n) = ((f \ominus g) \oplus g)(n) \quad (18)$$

Mathematical morphology function proposed by [9] is defined as follows,

$$MMF3(n) = (f(n) \circ (f \bullet g)(n) + f(n) \bullet (f \circ g)(n)) / 2 \quad (20)$$

$$MMF3_{dil}(n) = (MMF3 \oplus g)(n) \quad (21)$$

$$MMF3_{ero}(n) = (MMF3 \ominus g)(n) \quad (22)$$

$$MMF_{output}(n) = \begin{cases} MMF3_{dil}(n) - MMF3_{ero}(n) & \text{if } MMF3_{dil}(n) - MMF3_{dil}(n-1) > \delta \\ MMF3_{ero}(n) - MMF3_{dil}(n) & \text{if } MMF3_{ero}(n) - MMF3_{ero}(n-1) > \delta \end{cases} \quad (23)$$

Ref. [17] use the function corresponding to difference between erosion (f_{ero}) and dilation (f_{dil}) operators to identify the sudden changes of the signal while [18] uses the derived operator (MMF_{output}) from erosion (f_{ero}) and dilation (f_{dil}) operators. In [18], use of MM is demonstrated using mathematically synthesized signals while, in [17] use of MM is demonstrated with fault current waveforms obtained from

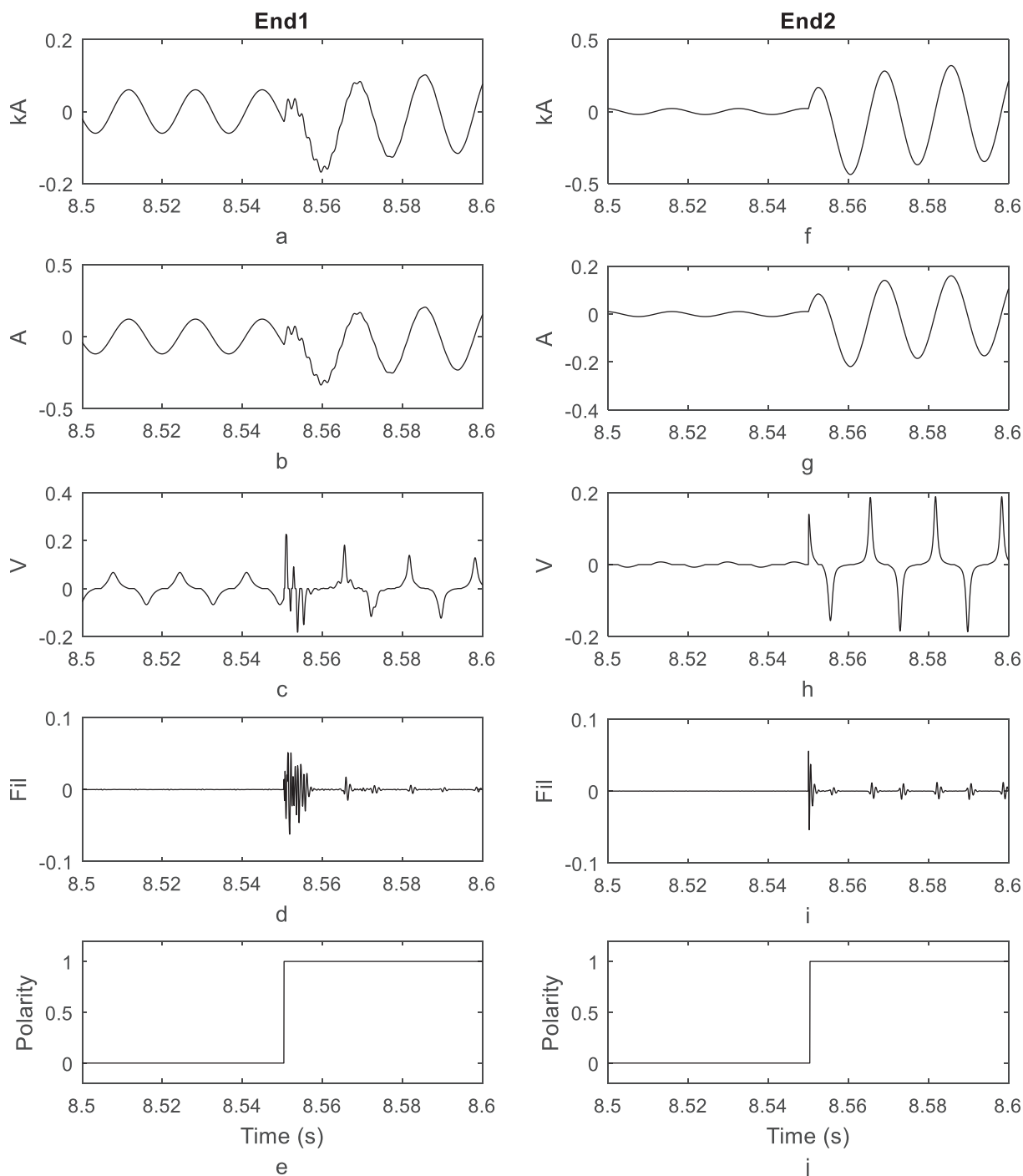


Fig. 13. Simulation results of internal fault.

simulations. In both the cases, clearly visible transients were present in the original input waveforms, and thus the corresponding outputs identified the edges. Figs. 10 and 11 show the response of two suggested methods for the experimental waveform used in Figs. 8 and 9 respectively. It is observed that, the plots of the functions defined in [18,17] were unable to detect a clear transient, although it detects the changes in low frequency components.

Comparison of ferrite coil response with the available signal processing methods shows the superiority of the proposed transient sensor compared to those methods. Although wavelet transform and MM are strong tools for signal processing, their performance may be limited by the signal noise and analogue to digital conversion precision.

6. Simulation of transient current polarity comparison based protection

In order to demonstrate the use of polarity detection sensor model developed in this paper, a simple 13.8 kV distribution feeder is simulated in PSCAD electromagnetic transient simulation program. Implementation is focused on the protection strategy proposed in [6]. As shown in Fig. 12 protection scheme consists of two transient polarity detection units. Simulation models of these polarity detection units were implemented in PSCAD based on the model described in Section 3. For an internal fault (a fault between the measuring points), the transient polarities must be the same, for the indicated current measurement directions [6]. Fig. 13 show the simulation results.

Fig. 13(a) and (f) shows the phase currents at two ends of the protected distribution line. Fig. 13(b) and (g) shows the outputs of the conventional current transformers located at the two ends of the distribution line. In this case, ferrite core coils are inserted to the secondary current path of the current transformers. Fig. 13(c) and (h) shows the response of the ferrite core coils at the two ends. Output of the ferrite core coils are filtered and polarities are determined using a threshold setting. Filtered ferrite coil waveforms at two ends is shown in Fig. 13(d) and (i). For this case both polarities are measured as positive as shown in Fig. 13(e) and (j), by the outputs indicating positive polarity transients. According to the a protection strategy proposed in [6], this indicates an internal fault.

7. Conclusion

In this a paper, a sensing arrangement is proposed for detecting high frequency transients in currents and their initial polarities. An open

Appendix A. Supplementary material

Supplementary data associated with this article can be found, in the online version, at <http://dx.doi.org/10.1016/j.ijepes.2018.03.027>.

Appendix B.

Design parameters of the Ferrite core coil

A	25	R	12.9×10^{-7}
α	10^{-4}	N_p	1
M_{Sat}	3.1×10^{-5}	N_s	5
c	10^{-3}	l	0.17
k	11.11×10^{-6}	A_c	1.7×10^{-4}

Design parameters PSCAD Test network

Distribution voltage level	13.8 kV
Line length	5 km
Distance to the fault from End1	2 km
CT ratio End1	100:1
CT ratio End2	100:1

References

- [1] "Publication: Status of Power System Transformation 2017". Available: < <https://www.iea.org/publications/freepublications/publication/status-of-power-system-transformation-2017.html> > . [accessed: 03-Nov-2017].
- [2] Haj-ahmed MA, Illindala MS. The influence of inverter-based DGs and their controllers on distribution network protection. *IEEE Trans Ind Appl Jul.* 2014;50(4):2928–37.
- [3] Chen B, Shrestha A, Ituzaro FA, Fischer N. Addressing protection challenges associated with Type 3 and Type 4 wind turbine generators. In: 2015 68th annual conference for protective relay engineers; 2015. p. 335–44.
- [4] E. Farantatos, U. Karaagac, H. Saad, and J. Mahseredjian, "Short-circuit current contribution of converter interfaced wind turbines and the impact on system protection," in 2013 IREP Symposium Bulk Power System Dynamics and Control - IX Optimization, Security and Control of the Emerging Power Grid, 2013, pp. 1–9.
- [5] Hooshyar A, Irvani R. Microgrid protection. *Proc IEEE Jul.* 2017;105(7):1332–53.
- [6] Pathirana A, Rajapakse A, Perera N. Development of a hybrid protection scheme for active distribution systems using polarities of current transients. *Electr Power Syst Res Nov.* 2017;152:377–89.
- [7] Guo Z, Yao J, Tan Z. Hilbert #x2013; Huang transform-based transient busbar protection algorithm. *Transm Distrib IET Gener* 2015;9(14):2032–9.
- [8] Kar S, Samantaray SR. Time-frequency transform-based differential scheme for microgrid protection. *Transm Distrib IET Gener Feb.* 2014;8(2):310–20.
- [9] Li X, Dyško A, Burt GM. Traveling wave-based protection scheme for inverter-dominated microgrid using mathematical morphology. *IEEE Trans Smart Grid Sep.* 2014;5(5):2211–8.
- [10] "SEL-T400L Time-Domain Line Protection | Schweitzer Engineering Laboratories," *selinc.com*. Available: < <https://selinc.com/products/T400L/?ref=v3-t400l> > . [accessed: 22-Sep-2017].
- [11] Huang Q, Jing S, Zhen W, Yi J. Innovative testing and measurement solutions for smart grid. John Wiley & Sons; 2016.
- [12] Perera N, Rajapakse AD. Design and hardware implementation of a modular transient directional protection scheme using current signals. *Transm Distrib IET Gener Jun.* 2012;6(6):554–62.
- [13] Bo ZQ, Redfern MA, Weller GC. Positional protection of transmission line using fault generated high frequency transient signals. *IEEE Trans Power Deliv Jul.* 2000;15(3):888–94.
- [14] Perera N, Rajapakse AD. Series-compensated double-circuit transmission-line protection using directions of current transients. *IEEE Trans Power Deliv Jul.* 2013;28(3):1566–75.
- [15] Bo Z, Weller G, Lomas T. A new technique for transformer protection based on transient detection. *IEEE Trans Power Deliv Jul.* 2000;15(3):870–5.
- [16] Pathirana V, McLaren PG. A hybrid algorithm for high speed transmission line protection. *IEEE Trans Power Deliv Oct.* 2005;20(4):2422–8.
- [17] Wu QH, Zhang JF, Zhang DJ. Ultra-high-speed directional protection of transmission lines using mathematical morphology. *IEEE Trans Power Deliv Oct.* 2003;18(4):1127–33.
- [18] Namdari F, Salehi M. High-speed protection scheme based on initial current traveling wave for transmission lines employing mathematical morphology. *IEEE Trans Power Deliv Feb.* 2017;32(1):246–53.
- [19] Douglass DA. Current transformer accuracy with asymmetric and high frequency fault currents. *IEEE Trans Power Appar Syst* 1981;PAS-100(3):1006–12. Mar.
- [20] Liu Y, Lin F, Zhang Q, Zhong H. Design and construction of a rogowski coil for measuring wide pulsed current. *IEEE Sens J Jan.* 2011;11(1):123–30.
- [21] Annakkage U, Piyadasa CKG, Gole A, Filizadeh S, Rajapakse A. Simultaneous Measurement Technique for Line Current, Geomagnetically Induced Currents (gic) and Transient Currents in Power Systems, WO/2015/070345; 22-May-2015.
- [22] Huang K. "Transient direction detector", US3986115 A; 12-Oct-1976.
- [23] Smith MN, Huang K. "Transient source and direction of propagation detector", US3986116 A; 12-Oct-1976.
- [24] Wilson PR, Ross JN, Brown AD. Modeling frequency-dependent losses in ferrite cores. *IEEE Trans Magn May* 2004;40(3):1537–41.
- [25] Jiles DC, Atherton DL. Theory of ferromagnetic hysteresis. *J Magn Magn Mater Sep.*

- 1986;61(1):48–60.
- [26] Annakkage UD, McLaren PG, Dirks E, Jayasinghe RP, Parker AD. A current transformer model based on the Jiles-Atherton theory of ferromagnetic hysteresis. *IEEE Trans Power Deliv* Jan. 2000;15(1):57–61.
- [27] Carpenter KH, Warren S. A wide bandwidth, dynamic hysteresis model for magnetization in soft ferrites. *IEEE Trans Magn Sep.* 1992;28(5):2037–41.
- [28] Nuwan Perera (University of Manitoba student), Detection, localization, and recognition of faults in transmission networks using transient currents; 2012.